

# Broad-Band Linearization of a Mach–Zehnder Electrooptic Modulator

Edward I. Ackerman, *Member, IEEE*

**Abstract**—Analog optical-link dynamic range in excess of 75 dB in a 1-MHz band has been achieved using specially designed electrooptic modulators that minimize one or more orders of harmonic and intermodulation distortion. To date, however, such “linearized” modulators have only enabled improved link dynamic ranges at frequencies below 1 GHz. Additionally, linearization across more than an octave bandwidth has required precise balancing of the signal voltage levels on multiple electrodes in a custom modulator, which represents a significant implementation challenge. In this paper, a link linearization technique that uses a standard Mach–Zehnder lithium–niobate modulator with only one RF and one dc-bias electrode to achieve broad-band linearization is discussed, resulting in a dynamic range of 74 dB in 1 MHz across greater than an octave bandwidth (800–2500 MHz). Instead of balancing the voltages on two RF electrodes, the modulator in this new link architecture simultaneously modulates optical carriers at two wavelengths, and it is the ratio of these optical carrier powers that is adjusted for optimum distortion canceling. The paper concludes by describing a second analogous link architecture in which it is the ratio of optical power at two modulated polarizations that is adjusted in order to achieve broad-band linearization.

**Index Terms**—Electrooptic modulation, intermodulation distortion, modeling, optical-fiber communication, wavelength division multiplexing.

## I. INTRODUCTION

ANALOG fiber-optic links assembled entirely from commercially available components can exhibit dynamic ranges that are adequate for many applications. For instance, one commercially available link,<sup>1</sup> in which the optical transmitter unit contains a directly modulated distributed-feedback (DFB) laser, has a very impressive third-order distortion-limited dynamic range of approximately 80 dB in 1 MHz if operated over any suboctave band between 10 MHz and 3 GHz (if operated over a frequency range in excess of one octave, second-order distortion limits this link’s dynamic range to approximately 70 dB in 1 MHz). Also, using a commercially available Mach–Zehnder external modulator operated at its quadrature bias voltage (where no even-order distortion is produced) in conjunction with a high-power laser and photodetector can yield dynamic range that is third-order distortion

limited to roughly 70 dB in 1 MHz across greater than an octave of bandwidth.

Some applications, such as broad-band fiber-optic remoting of RF antennas, can require greater link dynamic ranges than what these commercial links deliver. This need has driven analog fiber-optic link designers to pursue the development of modulators that are more linear than the standard Mach–Zehnder interferometric variety that is currently available.

## II. BACKGROUND: NONLINEARITY OF EXTERNAL INTENSITY MODULATION

In electrooptic intensity modulators, the input signal voltage modulates an optical waveguide’s refractive index via the linear electrooptic (Pockels) effect, and either a Mach–Zehnder interferometer or a directional coupler converts this optical phase modulation into intensity modulation. Unfortunately, either of these optical phase-to-intensity modulation conversion methods results in a nonlinear transfer function and, therefore, the input signal produces harmonic and intermodulation distortion at the link output.

It is possible to operate either a Mach–Zehnder or a directional-coupler type of electrooptic modulator around a dc-bias voltage at which the second derivative of the transfer function is zero; doing so eliminates distortion at the second harmonic and second-order intermodulation frequencies, causing third-order distortion products to dominate and, thus, limit the dynamic range to roughly 70 dB in a 1-MHz instantaneous bandwidth [1], [2]. To improve upon this, recent efforts have focused on the development of broad-band “linearized” modulators, in which third-order distortion is minimized at the same dc-bias voltage where no even-order distortion occurs. Fig. 1 shows three previously proposed broad-band linearized modulators (after [3]–[5]).

Two of the broad-band linearized modulators shown in Fig. 1 require that the RF signal be split and applied in precise proportion to two different RF electrodes. For efficient modulation at frequencies above 2 GHz or so, the modulator electrodes must be configured as transmission lines whose effective refractive index at RF frequencies closely matches the optical refractive index [6]. To achieve broad-band linearization at high frequencies, therefore, the RF characteristics of the modulator’s two traveling-wave electrodes (including RF attenuation per unit length, characteristic impedance, and guided-wave velocity as determined by the effective RF refractive index) must match each another over the entire band of interest. This RF signal balancing gets progressively more

Manuscript received March 26, 1999; revised July 12, 1999. This work was supported by the Defense Advanced Research Projects Agency under Air Force Contract F19628-95-C-0002.

The author was with the MIT Lincoln Laboratory, Lexington, MA 02420 USA. He is now with Photonic Systems Inc., Carlisle, MA 01741 USA.

Publisher Item Identifier S 0018-9480(99)08419-7.

<sup>1</sup>RF Fiber-Optic 1310-nm Small Integrated Transmitter Unit (SITU 1116) data sheet, Uniphase Telecommunications Products, Chalfont, PA, 1998.

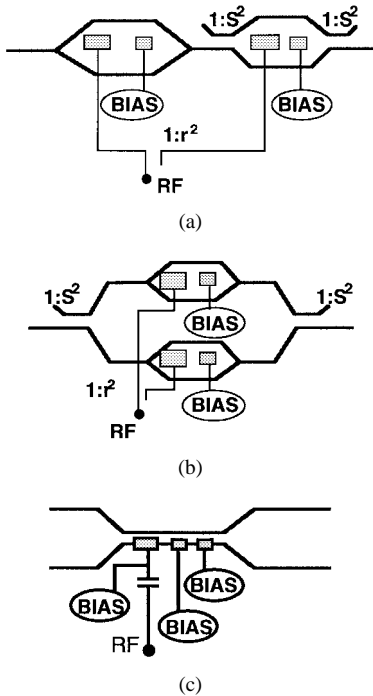


Fig. 1. Broad-band linearized electrooptic modulator configurations. (a) Series Mach-Zehnders [3]. (b) Parallel Mach-Zehnders [4]. (c) Modified directional coupler [5].

difficult to accomplish with increasing signal frequency and/or percentage bandwidth.

To my knowledge, the only broad-band (greater than an octave bandwidth) linearized electrooptic modulators proposed thus far that do not require application of the RF signal to more than one electrode are the modified directional coupler design shown in Fig. 1(c) and a similar Y-fed directional coupler design proposed more recently [7]. These devices are the same as a straightforward directional coupler modulator [2], except for the incorporation of two additional dc-biased electrodes that impose controlled mismatches in the propagation constants between the optical waveguides in the coupling region [5]. An analytical model [8] has shown that this modulator could achieve a dynamic range of 81 dB in 1 MHz across a broad band and at high frequencies, but only if the RF and optical refractive indexes were perfectly matched at all frequencies in the band. Any mismatch must be counteracted by “re-phasing,” which is splitting of the RF among multiple shorter electrode segments—leading back to the electrode characteristic-matching issue.

### III. TECHNICAL APPROACH

Fig. 2 shows the new broad-band linearization approach that uses a straightforward commercially available Mach-Zehnder modulator with a single traveling-wave RF electrode and a single dc-bias electrode. The Mach-Zehnder modulates two wavelengths of light simultaneously and, at the other end of the link, a wavelength-division multiplexer (WDM) routes the two modulated wavelengths to separate detectors whose outputs are combined in an RF hybrid coupler.

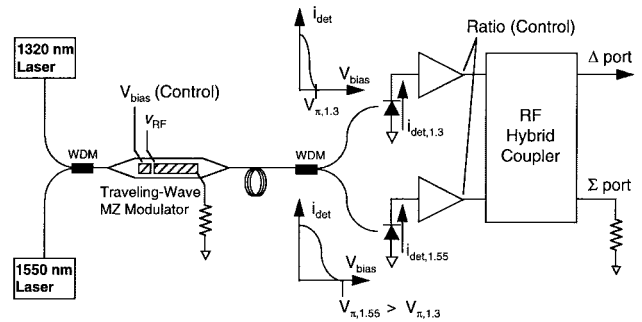


Fig. 2. New linearization architecture. Second- and third-order distortion are simultaneously minimized by precise control of the modulator bias and the ratio of optical power at the two optical wavelengths.

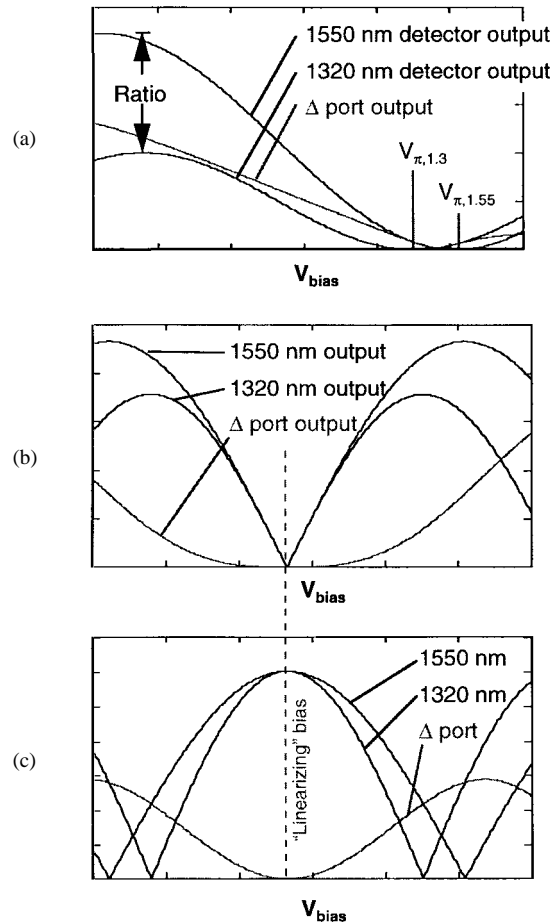


Fig. 3. (a) Photocurrent at the two individual detectors and the current at the  $\Delta$  output of the RF hybrid coupler as a function of the modulator bias. (b) Second derivative of the photocurrent at the individual detectors and at the  $\Delta$  output of the RF hybrid coupler as a function of the modulator bias. (c) Third derivative of the photocurrent at the individual detectors and at the  $\Delta$  output of the RF hybrid coupler as a function of the modulator bias.

The curves in Fig. 3(a) show how the photocurrents at the individual detectors vary with modulator bias voltage and how the current at the  $\Delta$  output of the RF hybrid coupler varies with modulator bias. Fig. 3(b) and (c) shows second and third derivatives of these curves, respectively. These plots reflect the case where the ratio of photocurrents is maintained such that, at the modulator bias where both detector outputs have zero even-order distortion, the detectors deliver equal levels of

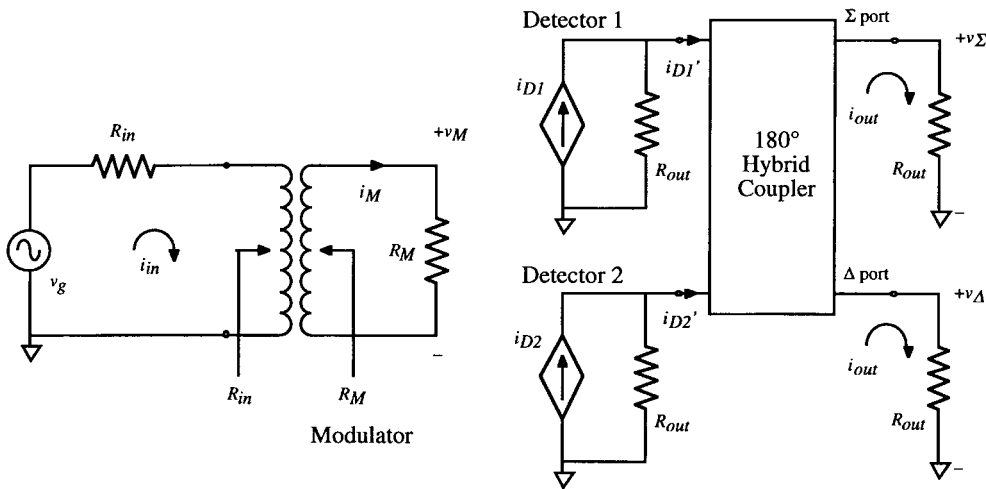


Fig. 4. Equivalent-circuit model of link employing the two-wavelength linearization architecture.

third-order distortion to the hybrid coupler. At this modulator bias and photocurrent ratio, the strongest distortion products present at the hybrid coupler's  $\Delta$  port are fifth order.

This new linearization architecture is analogous to the dual-parallel Mach-Zehnder modulator configuration shown in Fig. 1(b), in which the RF signal is split in a specific proportion between two Mach-Zehnders that are fed a single optical carrier that has also been split in a specific proportion. In the new configuration, only one Mach-Zehnder modulator is required because it has a different halfwave voltage ( $V_\pi$ ) at the two wavelengths; thus, an RF signal of magnitude  $v_M$  applied to the single electrode results in a different modulation depth  $v_M/V_\pi$  at the two wavelengths. This dual-wavelength approach also resembles one described by Johnson and Rousell, who canceled third-order (but not second-order) distortion by balancing two different *polarizations* of light that have different halfwave voltages in a lithium-niobate Mach-Zehnder modulator [9].

An important advantage imparted by this new multiple-wavelength linearization approach is that inexpensive commercially available fiber WDM's can be used to route the two modulated wavelengths of light to separate photodetectors whose outputs are combined electrically (as in Fig. 2). Wavelength multiplexing to separate detectors enables the use of electronic circuitry to precisely maintain the ratio of RF signal currents at the hybrid coupler inputs that results in distortion cancellation. The balancing circuit can be designed to adjust continually and automatically for unpredictable environmental factors such as stresses on the fiber that might induce variability in the relative losses at the two wavelengths [10]. The network containing the two detectors, balancing circuit, and hybrid coupler that combines the balanced signals is what would most likely set the upper limit to the bandwidth of a link of this type.

#### IV. THEORY

An equivalent-circuit model of a fiber-optic link employing the two-wavelength linearization approach is shown in Fig. 4. The modulator is assumed to have a single traveling-wave

electrode that is terminated in its characteristic impedance  $R_M$  and reactively impedance matched to the source resistance  $R_{in}$ . The two detectors are assumed to have photocurrents with RF components  $i_{D1}$  and  $i_{D2}$  proportional to the depth of modulation of the optical carriers at wavelengths  $\lambda_1$  and  $\lambda_2$ , respectively, and to have been resistively matched to the input ports of the hybrid coupler. Defining  $I_1$  and  $I_2$  as the two average photocurrents that occur when the modulator is biased for full transmission at both wavelengths (i.e., equal path length in the two arms of the Mach-Zehnder) it is possible to derive the RF small-signal gain, noise figure (NF), and distortion performance of the link.  $I_1$  and  $I_2$  depend on the two laser output powers and on the optical losses and detector responsivities at wavelengths  $\lambda_1$  and  $\lambda_2$ , respectively.

##### A. Small-Signal Gain

For small input RF signal power  $P_{in}$ , the RF signal powers at the  $\Sigma$  and  $\Delta$  output ports of the hybrid coupler are

$$P_{out,\Sigma}(\omega) = \frac{\pi^2}{32} \left[ \frac{I_1}{V_{\pi 1}} \sin\left(\frac{\pi V_{DC}}{V_{\pi 1}}\right) + \frac{I_2}{V_{\pi 2}} \sin\left(\frac{\pi V_{DC}}{V_{\pi 2}}\right) \right]^2 \times R_M R_{out} P_{in} \quad (1)$$

and

$$P_{out,\Delta}(\omega) = \frac{\pi^2}{32} \left[ \frac{I_1}{V_{\pi 1}} \sin\left(\frac{\pi V_{DC}}{V_{\pi 1}}\right) - \frac{I_2}{V_{\pi 2}} \sin\left(\frac{\pi V_{DC}}{V_{\pi 2}}\right) \right]^2 \times R_M R_{out} P_{in} \quad (2)$$

where  $V_{\pi 1}$  and  $V_{\pi 2}$  are the voltages required to impose 180° optical phase changes at the two wavelengths, and  $R_{out}$  is the impedance of the link output ports. Defining two ratios  $A$  and  $r$

$$A \equiv \frac{I_1}{I_2} \quad (3)$$

and

$$r \equiv \frac{V_{\pi 1}}{V_{\pi 2}} \quad (4)$$

the small-signal gain measured from the  $\Sigma$  and  $\Delta$  ports, respectively, are as follows:

$$G_{\Sigma} = \frac{I_1^2 \pi^2}{32V_{\pi 1}^2} \left[ \sin\left(\frac{\pi V_{DC}}{V_{\pi 1}}\right) + \frac{A}{r} \sin\left(\frac{\pi V_{DC}}{rV_{\pi 1}}\right) \right]^2 R_M R_{out} \quad (5)$$

and

$$G_{\Delta} = \frac{I_1^2 \pi^2}{32V_{\pi 1}^2} \left[ \sin\left(\frac{\pi V_{DC}}{V_{\pi 1}}\right) - \frac{A}{r} \sin\left(\frac{\pi V_{DC}}{rV_{\pi 1}}\right) \right]^2 R_M R_{out}. \quad (6)$$

### B. NF

The link's input thermal noise modulates the optical carriers the same way as the input signal does. Therefore, like the input signal, the input thermal noise is correlated at the output of the two photodetectors, and at the  $\Sigma$  or  $\Delta$  output of the hybrid coupler this noise at  $T = 290$  K has a power equal to  $kTBG_{\Sigma}$  or  $\Delta$ , where  $k$  is Boltzmann's constant and  $B$  is the receiver's instantaneous bandwidth. The modulator electrode's termination resistor generates thermal noise, but this does not efficiently modulate the light because it and the light are counter-propagating through the device. From either output port, the  $180^\circ$  hybrid coupler looks like a resistance  $R_{out}$  and, therefore, sends thermal noise power equal to  $kTB$  out of that port. All other noise powers detected by or generated in the two photodetectors are uncorrelated with respect to one another and, therefore, the total output noise power  $N_{out}$  from either output port is

$$N_{out} = kTBG + kTB + N_{out,RIN1} + N_{out,RIN2} + N_{out,shot1} + N_{out,shot2} \quad (7)$$

where  $N_{out,RIN1}$  and  $N_{out,shot1}$  are the photodetected RIN and shot noise powers contributed by the photodiode that detects wavelength  $\lambda_1$ , and likewise for  $\lambda_2$ . From each detector, half of the RIN and shot noise is channeled to the  $\Sigma$  output port, and the other half to the  $\Delta$  port, so that out of either port

$$\begin{aligned} N_{out,RIN1} &= \frac{1}{2} \left( \frac{i_{DC}^2 RIN_1 BR_{out}}{2} \right) \\ &= \frac{I_1^2}{16} \left[ 1 + \cos\left(\frac{\pi V_{DC}}{V_{\pi 1}}\right) \right]^2 RIN_1 BR_{out} \end{aligned} \quad (8)$$

$$N_{out,RIN2} = \frac{A^2 I_1^2}{16} \left[ 1 + \cos\left(\frac{\pi V_{DC}}{rV_{\pi 1}}\right) \right]^2 RIN_2 BR_{out} \quad (9)$$

$$\begin{aligned} N_{out,shot1} &= \frac{1}{2} \left( \frac{2qi_{DC}}{2} \right) BR_{out} \\ &= \frac{qI_1}{4} \left[ 1 + \cos\left(\frac{\pi V_{DC}}{V_{\pi 1}}\right) \right] BR_{out} \end{aligned} \quad (10)$$

and

$$N_{out,shot2} = \frac{qAI_1}{4} \left[ 1 + \cos\left(\frac{\pi V_{DC}}{rV_{\pi 1}}\right) \right] BR_{out}. \quad (11)$$

Therefore,

$$\begin{aligned} N_{out,\Sigma} &= kTBG_{\Sigma} + kTB + \frac{I_1^2}{16} \\ &\cdot \left( RIN_1 \left[ 1 + \cos\left(\frac{\pi V_{DC}}{V_{\pi 1}}\right) \right]^2 \right. \\ &\quad \left. + A^2 RIN_2 \left[ 1 + \cos\left(\frac{\pi V_{DC}}{rV_{\pi 1}}\right) \right]^2 \right) BR_{out} \\ &\quad + \frac{qI_1}{4} \left( 1 + \cos\left(\frac{\pi V_{DC}}{V_{\pi 1}}\right) \right) \\ &\quad \left. + A \left[ 1 + \cos\left(\frac{\pi V_{DC}}{rV_{\pi 1}}\right) \right] \right) BR_{out}. \end{aligned} \quad (12)$$

NF is defined as the signal-to-noise-ratio degradation through the link when the input noise is equal to  $kTB$ , i.e.,

$$NF \equiv \frac{N_{out}}{kTBG}. \quad (13)$$

Therefore, the two-wavelength link has the following NF:

$$\begin{aligned} NF_{\Sigma} &= 1 + \frac{1}{G_{\Sigma}} + \frac{I_1^2 R_{out}}{16kTG_{\Sigma}} \\ &\cdot \left( RIN_1 \left[ 1 + \cos\left(\frac{\pi V_{DC}}{V_{\pi 1}}\right) \right]^2 \right. \\ &\quad \left. + A^2 RIN_2 \left[ 1 + \cos\left(\frac{\pi V_{DC}}{rV_{\pi 1}}\right) \right]^2 \right) \\ &\quad + \frac{qI_1 R_{out}}{4kTG_{\Sigma}} \left( 1 + \cos\left(\frac{\pi V_{DC}}{V_{\pi 1}}\right) \right) \\ &\quad \left. + A \left[ 1 + \cos\left(\frac{\pi V_{DC}}{rV_{\pi 1}}\right) \right] \right). \end{aligned} \quad (14)$$

### C. Distortion

The output powers at the second harmonic and third-order-intermodulation distortion frequencies can be similarly derived from the Mach-Zehnder's simple sinusoidal transfer function

$$\begin{aligned} P_{out,\Sigma}(2\omega) &= \frac{1}{16} \left| \frac{I_1}{4} \left[ \cos\left(\frac{\pi V_{DC}}{V_{\pi 1}}\right) \pm \frac{A}{r^2} \cos\left(\frac{\pi V_{DC}}{rV_{\pi 1}}\right) \right] \right. \\ &\quad \times \left( \frac{\pi}{V_{\pi 1}} \right)^2 R_M P_{in} \\ &\quad \left. - \frac{I_1}{2} \left[ \cos\left(\frac{\pi V_{DC}}{V_{\pi 1}}\right) \pm \frac{A}{r^4} \cos\left(\frac{\pi V_{DC}}{rV_{\pi 1}}\right) \right] \right. \\ &\quad \left. \times \left( \frac{\pi}{V_{\pi 1}} \right)^4 (R_M P_{in})^2 + \dots \right|^2 R_{out} \end{aligned} \quad (15)$$

and

$$\begin{aligned}
& P_{\text{out},\Sigma}(2\omega_2 - \omega_1) \\
&= \frac{1}{16} \left| \frac{I_1}{16} \left[ \sin\left(\frac{\pi V_{\text{DC}}}{V_{\pi 1}}\right) \pm \frac{A}{r^3} \sin\left(\frac{\pi V_{\text{DC}}}{rV_{\pi 1}}\right) \right] \left(\frac{\pi}{V_{\pi 1}}\right)^3 \right. \\
&\quad \times (2R_M P_{\text{in}})^{(3/2)} - \frac{5I_1}{384} \left[ \sin\left(\frac{\pi V_{\text{DC}}}{V_{\pi 1}}\right) \right. \\
&\quad \quad \left. \pm \frac{A}{r^3} \sin\left(\frac{\pi V_{\text{DC}}}{rV_{\pi 1}}\right) \right] \\
&\quad \left. \times \left(\frac{\pi}{V_{\pi 1}}\right)^5 (2R_M P_{\text{in}})^{(5/2)} + \dots \right|^2 R_{\text{out}}. \quad (16)
\end{aligned}$$

#### D. Solution to Third-Order Linearization

Third-order distortion is minimized at the  $\Sigma$  port if the modulator bias voltage  $V_{\text{DC}}$  and the ratio  $A$  are chosen such that

$$\sin\left(\frac{\pi V_{\text{DC}}}{V_{\pi 1}}\right) + \frac{A}{r^3} \sin\left(\frac{\pi V_{\text{DC}}}{rV_{\pi 1}}\right) = 0 \quad (17)$$

and is instead minimized at the  $\Delta$  port if

$$\sin\left(\frac{\pi V_{\text{DC}}}{V_{\pi 1}}\right) - \frac{A}{r^3} \sin\left(\frac{\pi V_{\text{DC}}}{rV_{\pi 1}}\right) = 0. \quad (18)$$

Either way, these are the resulting expressions for gain, output noise, NF, and output power at the second harmonic and third-order intermodulation frequencies at the port where third-order linearization is achieved as shown in (19)–(22), at the bottom of this page, and

$$\begin{aligned}
& P_{\text{out}}(2\omega_2 - \omega_1) \\
&= \frac{25I_1^2 \pi^{10}}{73,728V_{\pi 1}^{10}} \left(1 - \frac{1}{r^2}\right)^2 \sin^2\left(\frac{\pi V_{\text{DC}}}{V_{\pi 1}}\right) R_{\text{out}} R_M^2 P_{\text{in}}^5. \quad (23)
\end{aligned}$$

Defining the input third-order intercept  $\text{IP3}_{\text{in}}$  as the input power  $P_{\text{in}}$  for which

$$P_{\text{in}} G = P_{\text{out}}(2\omega_2 - \omega_1) \quad (24)$$

it is clear that

$$\text{IP3}_{\text{in}} = 4\sqrt{\frac{3}{5}} \frac{V_{\pi 1}^2}{\pi^2 R_M} r. \quad (25)$$

The input third-order intercept is used in the calculation of spurious-free dynamic range (SFDR) as follows:

$$\text{SFDR} = \left(\frac{\text{IP3}_{\text{in}}}{kTB\text{NF}}\right)^{((p-1)/p)} \quad (26)$$

where  $p$  is the dominant order of distortion (for instance,  $p = 3$  if all even-order distortion is canceled and  $p = 5$  if third-order distortion is also canceled).

$$G = \frac{I_1^2 \pi^2}{32V_{\pi 1}^2} (1 - r^2)^2 \sin^2\left(\frac{\pi V_{\text{DC}}}{V_{\pi 1}}\right) R_M R_{\text{out}} \quad (19)$$

$$\begin{aligned}
N_{\text{out}} &= kTBG + kTB + \frac{I_1^2}{16} \left( \text{RIN}_1 \left[1 + \cos\left(\frac{\pi V_{\text{DC}}}{V_{\pi 1}}\right)\right]^2 + r^6 \text{RIN}_2 \frac{\sin^2\left(\frac{\pi V_{\text{DC}}}{V_{\pi 1}}\right)}{\sin^2\left(\frac{\pi V_{\text{DC}}}{rV_{\pi 1}}\right)} \left[1 + \cos\left(\frac{\pi V_{\text{DC}}}{rV_{\pi 1}}\right)\right]^2 \right) BR_{\text{out}} \\
&\quad + \frac{qI_1}{4} \left( 1 + \cos\left(\frac{\pi V_{\text{DC}}}{V_{\pi 1}}\right) + r^3 \left| \frac{\sin\left(\frac{\pi V_{\text{DC}}}{V_{\pi 1}}\right)}{\sin\left(\frac{\pi V_{\text{DC}}}{rV_{\pi 1}}\right)} \right| \left[1 + \cos\left(\frac{\pi V_{\text{DC}}}{rV_{\pi 1}}\right)\right] \right) BR_{\text{out}} \quad (20)
\end{aligned}$$

$$\begin{aligned}
\text{NF} &= 1 + \frac{1}{G} + \frac{I_1^2}{16kTG} + \left( \text{RIN}_1 \left[1 + \cos\left(\frac{\pi V_{\text{DC}}}{V_{\pi 1}}\right)\right]^2 + r^6 \text{RIN}_2 \frac{\sin^2\left(\frac{\pi V_{\text{DC}}}{V_{\pi 1}}\right)}{\sin^2\left(\frac{\pi V_{\text{DC}}}{rV_{\pi 1}}\right)} \left[1 + \cos\left(\frac{\pi V_{\text{DC}}}{rV_{\pi 1}}\right)\right]^2 \right) R_{\text{out}} \\
&\quad + \frac{qI_1}{4kTG} \left( 1 + \cos\left(\frac{\pi V_{\text{DC}}}{V_{\pi 1}}\right) + r^3 \left| \frac{\sin\left(\frac{\pi V_{\text{DC}}}{V_{\pi 1}}\right)}{\sin\left(\frac{\pi V_{\text{DC}}}{rV_{\pi 1}}\right)} \right| \left[1 + \cos\left(\frac{\pi V_{\text{DC}}}{rV_{\pi 1}}\right)\right] \right) R_{\text{out}} \quad (21)
\end{aligned}$$

$$\begin{aligned}
P_{\text{out}}(2\omega) &\approx \frac{I_1^2 \pi^4}{64V_{\pi 1}^4} \left| \frac{1}{2} \left[ \cos\left(\frac{\pi V_{\text{DC}}}{V_{\pi 1}}\right) - r \frac{\sin\left(\frac{\pi V_{\text{DC}}}{V_{\pi 1}}\right)}{\sin\left(\frac{\pi V_{\text{DC}}}{rV_{\pi 1}}\right)} \cos\left(\frac{\pi V_{\text{DC}}}{rV_{\pi 1}}\right) \right] - \left[ \cos\left(\frac{\pi V_{\text{DC}}}{V_{\pi 1}}\right) - \frac{1}{r} \frac{\sin\left(\frac{\pi V_{\text{DC}}}{V_{\pi 1}}\right)}{\sin\left(\frac{\pi V_{\text{DC}}}{rV_{\pi 1}}\right)} \cos\left(\frac{\pi V_{\text{DC}}}{rV_{\pi 1}}\right) \right] \right. \\
&\quad \left. \times \left(\frac{\pi}{V_{\pi 1}}\right)^2 (R_M P_{\text{in}}) \right|^2 R_{\text{out}} R_M^2 P_{\text{in}}^2; \quad (22)
\end{aligned}$$

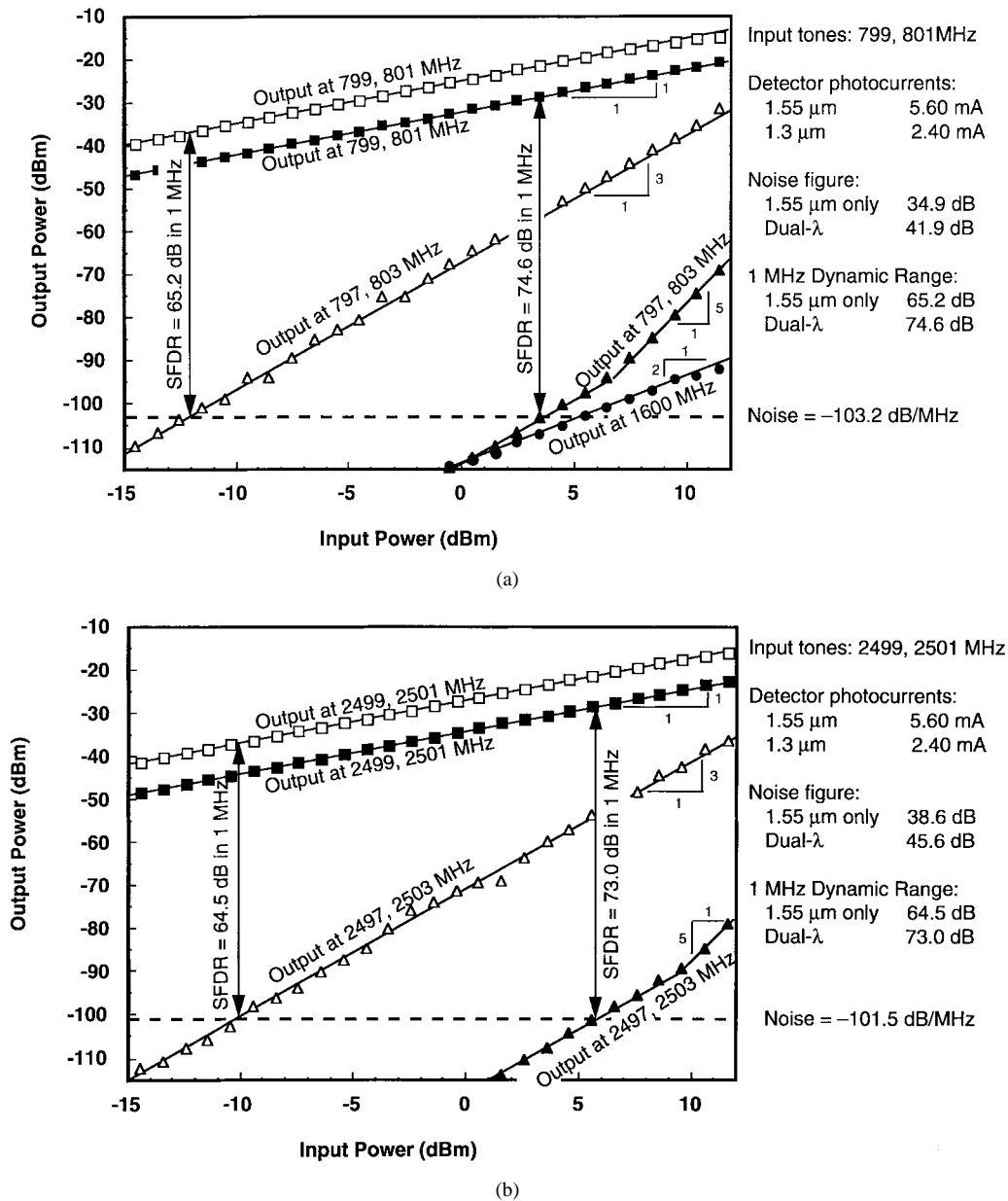


Fig. 5. (a) Link output noise (dashed line) and RF power measured at the fundamental (squares), second-order intermodulation (circles), and third-order intermodulation (triangles) frequencies as the RF input power at the fundamental frequencies (799 and 801 MHz) is varied. Hollow symbols represent the situation where only one of the wavelengths (1550 nm) is present, solid symbols represent two-wavelength operation at the proper ratio of detector photocurrents. (b) Same as (a), but with fundamental frequencies of 2499 and 2501 MHz. Modulator bias and photocurrent ratio settings are unchanged from the 799 and 801 MHz measurement.

### E. Solution to Third- and Second-Order (Broad-Band) Linearization

The modulator bias voltage  $V_{DC}$  can be chosen to minimize even-order distortion at both wavelengths. For zero even-order distortion,  $V_{DC}$  must satisfy the following equations:

$$\frac{\pi V_{DC}}{V_{\pi 1}} = \frac{2m+1}{2}\pi \quad (27)$$

and

$$\frac{\pi V_{DC}}{rV_{\pi 1}} = \frac{2n+1}{2}\pi, \quad \text{where } m, n \text{ are both integers.} \quad (28)$$

In practice, this means that the transfer functions for the outputs at the two optical wavelengths must both have an

inflection point at a voltage *exactly equal* to  $V_{DC}$ . It is possible, but not likely, that a reasonable bias voltage ( $|V_{DC}| \leq 20$  V) where this occurs can be found. However, it is quite likely that a reasonable bias voltage can be found that is merely *very close* to inflection points on both transfer-function curves, such that at this bias voltage even-order distortion is small enough that it does not impose a limit to the link's dynamic range. This issue is revisited in Section V. For now, it is assumed that there is a value of  $V_{DC}$  for which (27) and (28) are nearly satisfied, at which even-order distortion terms are sufficiently nulled so that (17) and (18) both approximate the following equation:

$$1 - \frac{A}{r^3} = 0. \quad (29)$$

Recall that  $A$  was defined as the ratio of detector photocurrents in response to the two wavelengths of light. This ratio can be continuously varied and set to any value between zero and infinity. Third-order distortion is minimized at one of the two output ports if

$$A = r^3. \quad (30)$$

Third-order distortion is minimized at the  $\Sigma$  port if  $m$  is odd and  $n$  is even, or if  $m$  is even and  $n$  is odd. Third-order distortion is minimized at the  $\Delta$  port if  $m, n$  are both odd or both even. Either way, the resulting link performance is as follows:

$$G = \frac{I_1^2 \pi^2}{32V_{\pi}^2} (1 - r^2)^2 R_M R_{out} \quad (31)$$

$$N_{out} = kTBG + kTB + \frac{I_1^2}{16} (RIN_1 + r^6 RIN_2) BR_{out} + \frac{qI_1}{4} (1 + r^3) BR_{out} \quad (32)$$

$$NF = 1 + \frac{1}{G} + \frac{I_1^2}{16kTG} (RIN_1 + r^6 RIN_2) R_{out} + \frac{qI_1}{4kTG} (1 + r^3) R_{out} \quad (33)$$

$$P_{out}(2\omega) = 0 \quad (34)$$

$$P_{out}(2\omega_2 - \omega_1) \approx \frac{25I_1^2 \pi^{10}}{73,728V_{\pi}^{10}} \left(1 - \frac{1}{r^2}\right)^2 R_{out} R_M^5 P_{in}^5 \quad (35)$$

$$IP3_{in} = 4\sqrt{\frac{3}{5}} \frac{V_{\pi}^2}{\pi^2 R_M} r \quad (36)$$

and

$$SFDR = \left( \frac{IP3_{in}}{kTB NF} \right)^{(4/5)}. \quad (37)$$

## V. DEMONSTRATION OF BROAD-BAND LINEARIZATION

Using only components of types that can be obtained commercially, a link in a configuration similar to the one shown in Fig. 2 was assembled. For the optical sources, an Nd:YAG laser with 200 mW output power at 1320 nm and an InGaAsP DFB laser with 30 mW output power at 1550 nm was used. Both lasers had polarization-maintaining fiber pigtailed. An erbium-doped fiber amplifier followed by an attenuator and filter (not shown in Fig. 2) was used to increase the available 1550-nm optical power. A WDM coupled the inputs at the two different wavelengths into one polarization-maintaining fiber so that both optical carriers could be fed into the modulator. The modulator used was a lithium-niobate Mach-Zehnder device with one traveling-wave RF electrode and one dc-bias electrode, and with very low  $V_{\pi}$ —about 2.4 V at 1320 nm. A second WDM demultiplexed the modulated optical carriers, each of which was routed to a separate InGaAs photodiode detector. The lengths of the fiber paths from the WDM to the two detectors were as carefully matched as closely as possible. Both detectors were followed with RF line stretchers and were then adjusted to equalize the group delay measured (using a network analyzer) from the modulator input to either input of the RF hybrid coupler.

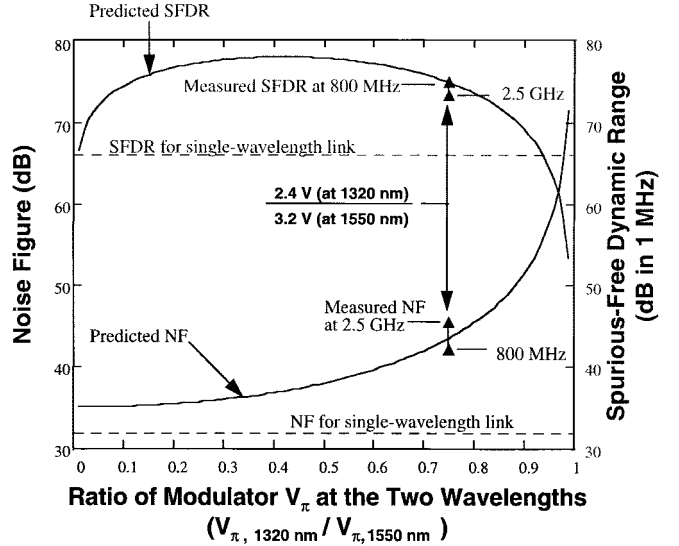


Fig. 6. Predicted SFDR in 1-MHz instantaneous bandwidth and NF for link employing two-wavelength linearization architecture (solid lines), as a function of the ratio  $r$  of the modulator's  $V_{\pi}$  at the two wavelengths. The SFDR and NF measured at 800 MHz and 2.5 GHz are also shown (triangles). Dashed lines show the SFDR and NF for an external modulation link with only a single modulated optical carrier (at 1550 nm).

Before attaching a broad-band hybrid coupler, the detector outputs were connected to separate RF spectrum analyzers, and the modulator input to an RF signal generator was set to 1 GHz. The modulator's dc-bias voltage was varied and minima at the second-harmonic frequency (2 GHz) were observed about every 2.4 V for the 1320 nm detector, and about every 3.2 V for the 1550 nm detector. Thus, for this modulator,  $r$  was approximately 0.75. At an experimentally determined modulator bias voltage of about +18 V, it happened that the 2-GHz output from either detector was very near one of its minima.

With the modulator bias fixed at this second-order minimum, the next step was to set the ratio of RF currents at the hybrid coupler input ports. Fig. 2 suggests one method involving amplifiers [10] for maintaining the two RF inputs to the hybrid coupler at the proper ratio for distortion cancellation. To achieve the proper ratio in the experiment reported here, a precision variable optical attenuator between the Nd:YAG laser and the 1320 nm input of the WDM was used. Feeding a two-tone RF input to the modulator, the 1320 nm carrier attenuation was varied until a minimum in the measured output power from the  $\Delta$  port of the hybrid coupler at the third-order intermodulation frequency was observed.

Varying the link input power at the two RF tones ( $f_1, f_2$ ), the link output power was measured at these tones, at one of the second-order intermodulation frequencies (the sum frequency  $f_1 + f_2$ ), and at the third-order intermodulation frequencies ( $2f_1 - f_2, 2f_2 - f_1$ ). Fig. 5(a) shows the measured results for 799 and 801 MHz input tones, along with the measured noise output in a 1-MHz instantaneous bandwidth. Fig. 5(b) shows results of the same measurement for input tones at 2499 and 2501 MHz (in which case, all second-order distortion falls out of band). In these plots, hollow squares and triangles represent measured data at the fundamental and

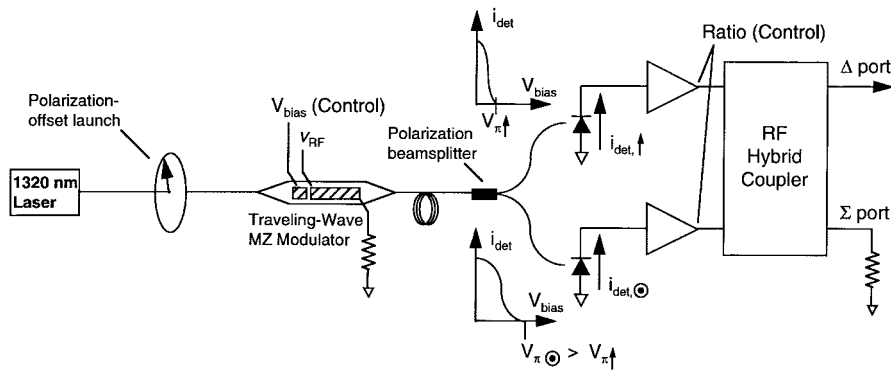


Fig. 7. Two-polarization broad-band linearization approach.

third-order intermodulation frequencies for the link with only the 1550-nm laser on (this yields better performance than the link with only the 1320-nm laser). When power at the second wavelength is present in proper proportion ( $A = r^3$ ) to the first wavelength, the output signal is reduced somewhat and third-order distortion is strongly suppressed, as shown by the solid squares and triangles, respectively. The measured second-order intermodulation distortion products are shown in Fig. 5(a) as solid circles. Note that the presence of any second-order distortion means that the bias voltage was not *exactly* at the inflection points of the modulator transfer-function curves for both optical wavelengths; however, the bias voltage was sufficiently close to inflection points on both transfer-function curves so that second-order distortion was not the order of distortion that limited the spur-free dynamic range of the link.

## VI. DISCUSSION

Fig. 5 has several features worth discussing. Firstly, and most significantly, the SFDR in a 1-MHz instantaneous bandwidth is 8–9 dB greater for the two-wavelength link, in accordance with its design. Secondly, the two-wavelength link suppresses second-order distortion incompletely, but to a degree sufficient to ensure that the dynamic range is third-order distortion limited. Thirdly, the same control settings (modulator bias and photocurrent ratio) yield linearization across more than an octave of bandwidth—i.e., from 800 MHz to 2.5 GHz. Fourthly, there is some noise-figure penalty associated with the linearization, which has been true for every broad-band linearized link that uses Mach–Zehnder modulators [11].

The increase in NF associated with this type of linearization is unfortunate, of course, but there is a way that it might be alleviated somewhat. Notice from (31) and (33) that each term in the expression for NF depends in a different way upon  $r$  (defined in (4) as the ratio of the modulator's  $V_{\pi}$  at  $\lambda_1$  to its  $V_{\pi}$  at  $\lambda_2$ ). This implies that there might be an optimum value of  $r$  at which the NF penalty is minimum. In Fig. 6, (31)–(37) have been used to plot the SFDR in a 1-MHz bandwidth along with the NF for the broad-band linearized link as a function of  $r$ . For the device parameters, the values measured for the devices in the experimental link were used, whose measured NF and SFDR are also shown in Fig. 6. Note that at  $r = 0.75$  (the experimental link's  $r$  value), there is a substantial (>10 dB)

NF penalty and an SFDR increase of only about 7 dB in a 1-MHz instantaneous bandwidth. The curves show, however, that a modulator with a  $V_{\pi}$  ratio of 0.4 at the two wavelengths would result in an SFDR increase of about 12 dB with an associated NF penalty of only 5 dB or so.

How to achieve the optimum  $V_{\pi}$  ratio? Fig. 7 shows a similar, but somewhat improved link linearization approach in which the modulator is fed two orthogonal polarizations of light. Since the strength of the electrooptic effect in lithium niobate is different for the two orthogonal polarizations, the  $\Delta$  output of the hybrid coupler can have zero second- and third-order distortion at one dc-bias voltage given a specific distribution of optical powers in these two polarizations. All equations given in Section IV hold in this case, but  $V_{\pi 1}$  and  $V_{\pi 2}$  now correspond to the modulator's halfwave voltages at the two polarizations of light at a single wavelength. In lithium niobate the ratio  $r$  of  $V_{\pi}$ 's at the two polarizations is likely to be closer to the optimum value of 0.4, shown in Fig. 6, indicating that this configuration could give better performance than the two-wavelength approach. Additionally, an obvious and very attractive feature of the two-polarization approach is that it requires only one laser.

Johnson and Roussel [9] pursued a similar two-polarization linearization approach, but did not use a polarization beamsplitter to route the two modulated polarizations to two separate photodetectors. Encountering trouble achieving the correct ratio of optical powers at the two polarizations, they had to compensate by adjusting the modulator bias. Thus, they were able to cancel only third-order distortion (which is not sufficient for enhancing the SFDR of a link that must operate across a bandwidth exceeding one octave).

Except for the polarization beamsplitter and custom polarization-maintaining fiber splice at approximately  $45^\circ$  off-axis, assembly of the link in Fig. 7 required only a subset of the components used in the two-wavelength linearization experiment. Initial measurements of the two-polarization link's performance have yielded results close to what Fig. 6 predicts for the modulator's measured  $r$  value of 0.33 for the two polarizations.  $NF = 38 \pm 1.5$  dB and  $SFDR = 74 \pm 1$  dB across the 800–2500-MHz band were measured.

One final feature worth pointing out is as follows. If either the two-wavelength or two-polarization link is used in a system operating over less than an octave bandwidth,

then linearization involves minimizing only the third-order distortion. Therefore, instead of having to satisfy (27)–(29) to achieve broad-band linearization—which completely specify both the ratio  $A$  and the modulator bias  $V_{DC}$ —it is only necessary to satisfy either (17) or (18)—in which for any modulator bias  $V_{DC}$ , there is a corresponding value of the ratio  $A$  that results in suboctave-bandwidth (i.e., third order) linearization. The modulator could thus be operated at a bias that minimizes NF (i.e., “low biasing” [12], [13]) and the optical power at the two wavelengths or polarizations could still be maintained at a ratio  $A$  that cancels the third-order distortion. Since the modulator has a single traveling-wave electrode, a suboctave link of this type would still have the advantage of linearizing at higher frequencies than what has been previously demonstrated.

## VII. SUMMARY

Proposals for linearization of a fiber-optic link across more than an octave bandwidth have required precise balancing of the signal voltage levels on multiple electrodes in a custom modulator, which represents a significant implementation challenge. A new link linearization method that uses a standard Mach-Zehnder lithium-niobate modulator with only one RF and one dc-bias electrode to linearize across greater than an octave bandwidth has been described. Instead of balancing the voltages on two RF electrodes, this new technique uses the standard traveling-wave electrode to modulate two optical carriers, and it is the ratio of these optical carrier powers that is adjusted for distortion canceling.

## ACKNOWLEDGMENT

The author is grateful to W. Burns, Naval Research Laboratory, Washington, DC, for the modulator loans, to G. Betts, C. Cox and P. Haddad for helpful discussions, and to S. Henion, H. Roussel, M. Taylor, and J. Vivilecchia for technical assistance. The views expressed in this paper are those of the author and do not reflect the official policy or position of the U.S. Government.

## REFERENCES

- [1] I. Kaminow, “Optical waveguide modulators,” *IEEE Trans. Microwave Theory Tech.*, vol. 23, pp. 57–69, Jan. 1995.
- [2] S. Kurazono, K. Iwasaki, and N. Kumagai, “A new optical modulator consisting of coupled optical waveguides,” *Electron. Commun. Japan*, vol. 55, pp. 103–109, Jan. 1972.

- [3] H. Skeie and R. Johnson, “Linearization of electro-optic modulators by a cascade coupling of phase modulating electrodes,” *Proc. SPIE-Int. Soc. Opt. Eng.*, vol. 1583, pp. 153–164, Mar. 1991.
- [4] S. Korotky and R. DeRidder, “Dual parallel modulation schemes for low-distortion analog optical transmission,” *IEEE J. Select. Areas Commun.*, vol. 8, pp. 1377–1381, Sept. 1990.
- [5] M. Farwell, Z. Lin, E. Wooten, and W. Chang, “An electrooptic intensity modulator with improved linearity,” *IEEE Photon. Technol. Lett.*, vol. 3, pp. 792–795, Sept. 1991.
- [6] R. Alferness, “Waveguide electrooptic modulators,” *IEEE Trans. Microwave Theory Tech.*, vol. MTT-30, pp. 1121–1137, Aug. 1982.
- [7] R. Tavlykaev and R. Ramaswamy, “Highly linear Y-fed directional coupler modulator with low intermodulation distortion,” *J. Lightwave Technol.*, vol. 17, pp. 282–290, Feb. 1999.
- [8] U. Cummings and W. Bridges, “Bandwidth of linearized electrooptic modulators,” *J. Lightwave Technol.*, vol. 16, pp. 1482–1490, Aug. 1998.
- [9] L. Johnson and H. Roussel, “Reduction of intermodulation distortion in interferometric optical modulators,” *Opt. Lett.*, vol. 13, p. 928, Oct. 1988.
- [10] C. Cox and A. Yee, “RF gain stabilization of a directly modulated optical link using detector current normalization,” in *IEEE Microwave Theory Tech. Symp. Dig.*, May 1994, pp. 1117–1120.
- [11] W. Bridges and J. Schaffner, “Distortion in linearized electrooptic modulators,” *J. Lightwave Technol.*, vol. 43, pp. 2184–2197, Sept. 1995.
- [12] M. Farwell, W. Chang, and D. Huber, “Increased linear dynamic range by low biasing the Mach-Zehnder modulator,” *IEEE Photon. Technol. Lett.*, vol. 5, pp. 779–782, July 1993.
- [13] E. Ackerman, S. Wanuga, D. Kasemset, A. Daryoush, and N. Samant, “Maximum dynamic range operation of a microwave external modulation fiber-optic link,” *IEEE Trans. Microwave Theory Tech.*, vol. 41, pp. 1299–1306, Aug. 1993.



**Edward I. Ackerman** (S’86–M-87) received the B.S. degree in electrical engineering from Lafayette College, Easton, PA, in 1987, and the M.S. and Ph.D. degrees in electrical engineering from Drexel University, Philadelphia, PA, in 1989 and 1994, respectively.

From 1989 to 1994, he was a Microwave Photonics Engineer at Martin Marietta’s Electronics Laboratory, Syracuse, NY. From 1995 to 1999, he was a Member of the Technical Staff at the MIT Lincoln Laboratory, Lexington, MA. He is currently Vice President of Research and Development for Photonic Systems Inc., Carlisle, MA, where he develops high-performance analog photonic links for microwave communications and antenna remoting applications. He has authored or co-authored over 50 technical papers on the subject of analog photonic subsystem performance modeling and optimization.